Growth of pentacene on clean and modified gold surfaces

Daniel Käfer, Lars Ruppel, and Gregor Witte[*]

Physikalische Chemie I, Ruhr-Universität Bochum, 44780 Bochum, Germany
(Received 30 August 2006; revised manuscript received 5 December 2006; published 9 February 2007)

The growth and evolution of pentacene films on gold substrates have been studied. By combining complementary techniques including scanning tunneling microscopy, atomic force microscopy, scanning electron microscopy, near-edge x-ray-absorption fine structure, and x-ray diffraction, the molecular orientation, crystalline structure, and morphology of the organic films were characterized as a function of film thickness and growth parameters (temperature and rate) for different gold substrates ranging from Au(111) single crystals to polycrystalline gold. Moreover, the influence of precoating the various gold substrates with self-assembled monolayers (SAM's) of organothiols with different chemical terminations has been studied. On bare gold the growth of pentacene films is characterized by a pronounced dewetting while the molecular orientation within the resulting crystalline three-dimensional islands depends distinctly on the roughness and cleanliness of the substrate surface. After completion of the first wetting layer where molecules adopt a planar orientation parallel to the surface the molecules continue to grow in a tilted fashion: on Au(111) the long molecular axis is oriented parallel to the surface while on polycrystalline gold it is upstanding oriented and thus parallels the crystalline orientation of pentacene films grown on SiO_2. On SAM pretreated gold substrates the formation of a wetting layer is effectively suppressed and pentacene grows in a quasi-layer-by-layer fashion with an upstanding orientation leading to rather smooth films. The latter growth mode is observed independently of the chemical termination of the SAM's and the roughness of the gold substrate. Possible reasons for the different growth mechanism as well as consequences for the assignment of spectroscopic data of thin pentacene film are discussed.

I. INTRODUCTION

Organic semiconductors have recently attracted considerable attention because of their promising potential for fabrication of thin-film organic electronic devices.[1,2] Among the various organic semiconductors investigated so far,[3] polyacenes such as pentacene ($C_{22}H_{14}$) are of particular interest because these materials reveal remarkably high charge carrier mobilities in their crystalline phase. Moreover, their ability to form highly ordered (poly)crystalline films allows the fabrication of thin-film organic field-effect transistors (OFET's) with excellent device properties.[4,5]

In its crystalline bulk structure pentacene forms a triclinic lattice with a characteristic layered structure consisting of (001) planes. Within each layer the molecules are upstanding oriented and adopt a face-on-edge herringbone arrangement[6,7] which is a common packing motive found in most planar polycyclic hydrocarbons (see Fig. 1). Related to this molecular structure also a pronounced anisotropy is obtained for the charge carrier mobility[8] which has been attributed to differences in the orbital overlap of neighbored molecules along the various crystallographic directions.[9] Therefore a precise control of the molecular packing and orientation in thin films is of vital interest for an optimization of thin-film OFET's and has become a topic of intense research.[10]

Frequently, it is found that the structure of organic films is mainly governed by the first monolayer which in turn depends on the interplay between the mutual interaction among the organic molecules and their interaction with the substrate surface. For example, in the case of insulator substrates such as SiO_2, which is commonly used as gate dielectric in

OFET's, pentacene molecules are only weakly adsorbed and grow in an upstanding orientation, forming islands with a (001) orientation.[11] A closer inspection showed further that upon room-temperature deposition initially a thin-film phase develops which is characterized by a slightly expanded interlayer-spacing[12,13] attributed to a nearly upright molecular orientation. A rather different scenario is observed upon initial film growth of pentacene and other planar aromatic molecules on many metal surfaces. Due to additional chemical interactions of the molecular π system with most metallic substrates the molecules are chemisorbed with their aromatic plane parallel to the surface (see, e.g., Refs. 10 and 14 and references therein). However, with increasing film thickness such an orientation is not maintained and instead a molecular reorientation has been observed upon further deposition of pentacene on various crystalline metal surfaces.[15–17] A similar reorientation was also found for thin films of perylene,[18] thus indicating some limitations of a simple template-mediated growth. Instead a characteristic dewetting and is-
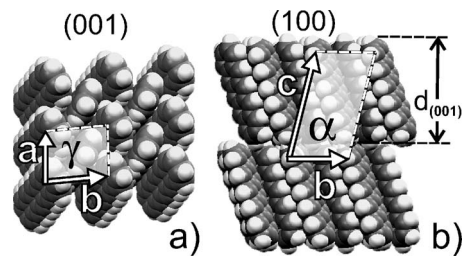

FIG. 1. Molecular ordering of pentacene in the triclinic bulk crystal structure (Ref. 6) showing (a) the (001) plane and (b) the (100) plane together with the interlayer spacing $d_{(001)} = 14.1$ Å.

land formation is frequently observed which appears to be a quite general phenomenon during growth of organic films on metals.[16–23]

Another important factor that determines the properties of organic electronic devices is the electronic coupling at the electrodes which affects, for example, the charge carrier injection. In the case of pentacene-based thin-film transistors gold is a commonly used electrode material because the reasonable energy-level alignment between the highest occupied molecular orbital (HOMO) and the Fermi level of gold provides a small injection barrier for holes.[24–26] Driven by the technical relevance of this pentacene/gold interface its geometrical microstructure has been characterized in great detail using scanning tunneling microscopy (STM) and various ordered (sub)monolayer phases with a planar adsorption geometry were identified.[27,28] In a later STM study Kang and Zhu reported a very similar molecular ordering also beyond the first monolayer which they attributed to a cofacial π stacking.[29] However, the fact that a long-range ordering was observed after annealing of multilayer films at temperatures where sublimation of pentacene already takes place has raised some concerns about this assignment. In fact by employing near-edge x-ray absorption fine structure (NEXAFS) spectroscopy and atomic force microscopy (AFM) to determine the molecular orientation and the film morphology we have demonstrated previously that such pentacene films reveal at room temperature a pronounced dewetting and form islands where molecules adopt an upstanding orientation.[17] In a recent study Hu *et al.* have shown that the formation of a chemisorbed pentacene wetting layer with a planar adsorption geometry can be suppressed by first coating the gold surface with a self-assembled monolayer (SAM). Based on NEXAFS and x-ray diffraction (XRD) measurements they demonstrated that subsequently deposited pentacene grows in an upstanding orientation.[30] On the other hand, for multilayer films of pentacene grown on bare Au/Si substrates they observed an orientation of the molecular planes nearly parallel to the substrate surface. While SAM's and other molecular layers are well known to modify surface properties[31,32] and have been successfully used to also influence the growth of organic films,[33–35] the different molecular structures reported for pentacene films of bare gold surfaces are yet not consistent.

A fundamental understanding of organic film growth on metals and the particular importance of gold as electrode material for organic electronics have stimulated the present growth study. To resolve the apparent differences reported for pentacene films on gold and to study the influence of surface properties such as roughness and cleanliness on the resulting film structure various gold substrates, including Au(111) single crystals and (111)-textured and polycrystalline gold films, have been examined. For comparison some of the various gold surfaces have also been chemically modified by coating with SAM's of different functionality, and moreover, the influence of deposition rate and substrate temperature on the resulting film structure was studied for various film thicknesses. The structure and morphology of the pentacene films and the molecular orientation were characterized by combining various scanning probe microscopy techniques (STM, AFM) and scanning electron microscopy (SEM) with XRD and NEXAFS.

The paper is organized in the following way. First, we provide a description of the experimental setup. In Sec. III we report at first the film morphologies observed upon room-temperature deposition on clean and SAM-coated gold substrates, followed by growth experiments for different deposition rates and temperatures. Next, the analysis of the molecular orientation derived from NEXAFS measurements for the different films and the diffraction patterns of the crystalline pentacene films are presented. After a discussion the paper closes with some concluding remarks.

II. EXPERIMENTAL SECTION

For the present growth study different types of gold substrates have been examined comprising a Au(111) single crystal and various gold films. The gold films were prepared by evaporating (150 nm) gold (99.995%, Chempur) under high-vacuum conditions ($<10^{-7}$ mbar) onto Si-wafer or mica substrates at room temperature or at 580 K, respectively. Before deposition the freshly cleaved mica sheets had been heated at 580 K for about 24 h under vacuum conditions to remove residual crystal water while the (100)-oriented and polished silicon wafers were first coated with a 5-nm titanium adhesion layer. The thickness and deposition rate (10 Å/s) were monitored using a quartz crystal microbalance. After deposition, the gold/mica substrates were flame annealed in a butane/oxygen flame prior to the growth experiments. This procedure yielded high-quality Au films with flat terraces of several 100 nm exhibiting a (111) surface orientation.

All pentacene films have been prepared under ultrahigh-vacuum (UHV) conditions and were primarily characterized *in situ*. A combined SEM-STM UHV microscope (Jeol JSPM 4500S) was used to characterize the molecular ordering and film morphology. This instrument facilitates the acquisition of SEM micrographs under true UHV conditions and especially allows a tip approach onto the sample under SEM control.[36] Due to the grazing incidence of the electron column in this instrument, the acquired SEM images reveal a characteristic distortion which has been corrected based on reference data recorded for squared transmission electron microscopy (TEM) grids. For all STM experiments freshly etched tungsten tips were used.

The NEXAFS measurements were performed at the synchrotron storage ring BESSY II in Berlin (Germany) at the dipole beamline HE-SGM using an end-station described in details elsewhere.[37] All NEXAFS measurements were carried out with linear polarized synchrotron light with a polarization factor of $P \approx 85\%$ and an energy resolution of about 100 meV at the C K edge. The NEXAFS spectra were recorded in a partial electron yield mode using a homemade electron detector based on a channel plate and a retarding field of -150 V. The energy calibration of all NEXAFS spectra is carried out by recording simultaneously with each spectrum the photocurrent of a carbon contaminated gold grid in the incident beam. This signal reveals a characteristic absorption peak at a photon energy of 284.9 eV,[38] which had been cross-calibrated by means of a graphite sample. The NEXAFS raw data have been normalized in a multistep pro-

cedure by considering the incident photon flux measured by the photocurrent on the grid and the background signal of the clean substrate (for details see Ref. 37).

Additional films were prepared in a third multitechnique instrument[39] which further allows sample characterizations by means of UV-photoelectron spectroscopy (UPS) and low-energy electron diffraction (LEED). All three UHV instruments are additionally equipped with a load-lock system, a sputter gun for sample cleaning, a x-ray photoelectron spectrometer (XPS), and homebuilt Knudsen-cell-type evaporators. Pentacene was deposited at normal incidence onto the gold samples from a glass crucible. Before film deposition the newly loaded pentacene (Fluka, nominal purity 97%) was thoroughly degassed under UHV conditions to remove the more volatile pentacenequinone species. Additional laser desorption ionization time-of-flight mass spectroscopy (LDI-TOF) measurements (cf. Ref. 40, not shown) yielded a remaining level of pentacene oxide impurities of less than 0.5%. To maintain a constant flux the source temperature was stabilized within ±1 K at typical operation temperatures of 500–560 K, yielding growth rates of 0.1–20 nm/min as monitored by a quartz microbalance.

The morphology of the pentacene films was further characterized *ex situ* by AFM (Jeol JSPM 4210, operated in tapping mode), and additional SEM measurements which were carried out in a separate microscope (LEO/Zeiss, 1530 Gemini FESEM, operated at 5–10 keV).

$\theta/2\theta$ measurements were used to determine the crystallographic phases of the pentacene films. The data were obtained from a x-ray diffractometer (Bruker, D8 Advance powder diffractometer) operated in Bragg-Brentano geometry using Cu $K\alpha$ radiation ($\lambda = 1.5405$ Å) while rotating the sample around the surface normal.

In addition the growth of pentacene films on chemically modified gold surfaces has been studied. For this purpose some of the gold surfaces had been precovered by self assembled monolayers of various organothiols including pure alkanethiols [C_n, $H_3C(CH_2)_{n-1}SH$, $n = 10$, 12, and 18] and differently terminated alkanethiols such as mercaptoundecanic acid [AcT, $HOOC(CH_2)_{10}SH$] and hemicosafluoro-dodecane-1-thiol [FT, $F_3C(CF_2)_9(CH_2)_2SH$] as well as an aromatic terphenyl-4-butanethiol [TP4, $C_6H_5(C_6H_4)_2(CH_2)_4SH$]. These monolayer films were prepared by immersion of freshly prepared gold films for about 24 h in 0.1–1 mM ethanolic solutions followed by careful rinsing with pure ethanol, a procedure which yields well ordered SAM's.[31,32]

III. RESULTS

A. Clean gold surfaces

At first the initial growth of pentacene was studied by characterizing thin films of about 2–3 nm deposited at room temperature onto gold/mica substrates. Before pentacene deposition the freshly prepared gold films were flame annealed and again heated in the UHV system at 500–600 K. A typical SEM micrograph which was recorded after deposition of nominal 3 nm pentacene with a rate of 1 nm/min is
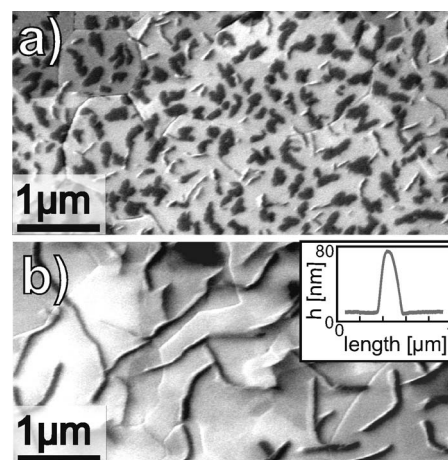

FIG. 2. SEM micrographs of a 3-nm pentacene film grown at room temperature on a Au/mica substrate (a) directly after deposition and (b) 12 h later. The inset reveals a line scan derived from AFM measurements across a ropelike pentacene island.

shown in Fig. 2(a). Individual islands with lateral dimensions of 100–300 nm are formed and appear as dark patches. This contrast can be related to an attenuation of secondary electrons from the gold surface through the pentacene islands. Surprisingly, the size and shape of such islands changed completely when keeping the sample in the UHV system at room temperature. After about 12 h rather long, ropelike islands are formed as displayed in Fig. 2(b) while no further morphological changes were observed at least within the next 48 h. *Ex situ* AFM measurements yielded a typical height of these features of 60–80 nm while no lower islands were observed, thus reflecting an extreme dewetting. Additional SEM measurements indicated that the morphology of these islands does not further change when keeping the sample in air for a period of several weeks. A closer inspection of the SEM micrograph indicates that the elongated islands are not aligned along the grain boundaries of the gold substrate, which are also visible as bright edges, but instead frequently grow across such boundaries.

Next we have examined the morphology of a thin pentacene film (about 2 nm) grown on a Au(111) single crystal which had been cleaned thoroughly before the deposition by repeated cycles of sputtering and annealing. Again the appearance of elongated islands was found. However, in contrast to the gold/mica substrates studied before they are formed immediately upon deposition and are significantly shorter. From *ex situ* AFM measurements typical island heights of 40–60 nm were obtained. A further analysis of the azimuthal orientation of the pentacene island suggests that they are not randomly distributed. The comparison with the substrate azimuth directions determined from LEED measurements of the clean gold surface indicates a prevailing aligning along the $\langle 1\bar{1}0\rangle$ directions as indicated in Fig. 3(a).

To elucidate the different kinetics of dewetting observed for the two gold substrates they have been further analyzed by photoelectron spectroscopy. While the differently prepared gold surfaces appeared to be clean according to the XPS data significant differences were found in the corre-
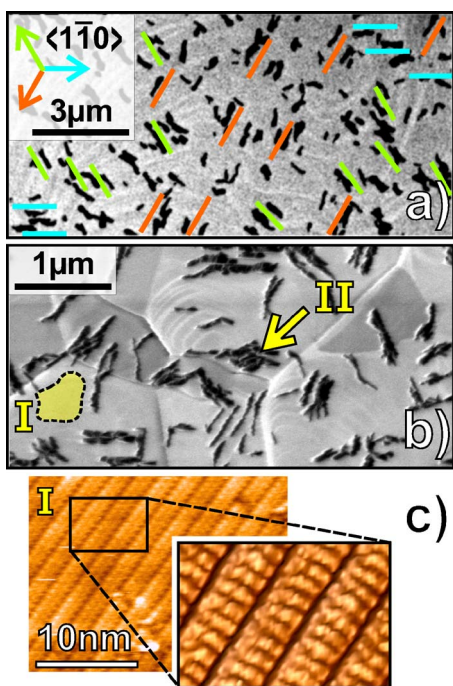
FIG. 3. (Color online) SEM micrographs of 2-nm pentacene films grown at room temperature on (a) clean Au(111) and (b) clean Au/mica surfaces together with the superimposed $\langle 1\bar{1}0 \rangle$ azimuth directions of the substrate in panel (a). Panel (c) displays STM data ($U_{sample}=-2$ V, $I=15$ pA) of the pentacene monolayer (indicated as I) between the islands (indicated as II).
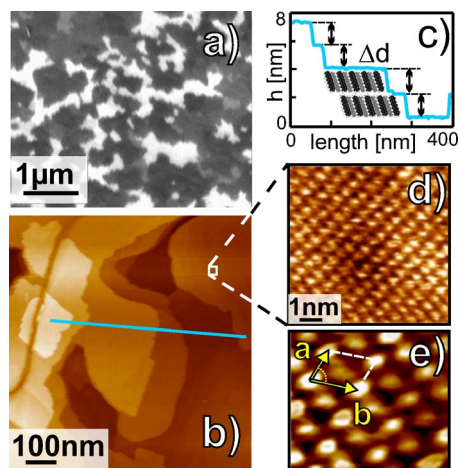

FIG. 4. (Color online) Morphology of a 4-nm pentacene film grown at room temperature on a decanethiol covered Au(111)/mica substrate. The SEM micrograph (a) displays the presence of extended pentacene islands consisting of smooth terraces planes with a step height of $\Delta d=1.6\pm0.3$nm as derived from STM data [line scan in panels (b) and (c)]. Panels (d) and (e) display molecularly resolved STM images ($U_{sample}=-2$ V and $I=15$ pA) which reveal a close-packed arrangement of pentacene molecules with a herringbone ordering in such planes together with the unit cell [panel (e)].

sponding work function of the samples. For the UHV-cleaned Au(111) surface a work function of about 5.2 eV was measured whereas only a value of 4.7 eV (and even 4.3 eV before heating) was obtained for the Au/mica sample. These data indicate striking differences in the surface cleanliness for both preparations which is difficult to detect by XPS. Based on these results all subsequent growth studies on Au/mica were carried out after the substrates had been thoroughly cleaned by repeated cycles of sputtering and annealing until they also revealed a work function of more than 5.1 eV. Corresponding STM measurements confirm an excellent surface quality and reveal the presence of atomically flat terraces extending over several 100 nm which exhibit the atomic structure of Au(111) terraces with the characteristic herringbone reconstruction (not shown). In fact the subsequent growth of pentacene on such cleaned Au/mica substrates parallels the situation observed before for a clean Au(111) single crystal surface and leads to a similar, immediate dewetting and formation of elongated islands as depicted in Fig. 3(b). In the further course of experiments STM was employed to characterize the microstructure of the pentacene films. First, the bright parts between the distinct pentacene islands [denoted as I in Fig. 3(b)] were studied. High-resolution STM data reveal a well-ordered molecular structure with characteristic rows separated by 15.5 ± 0.5 Å and a periodicity of 5.7 ± 0.3 Å along such rows as displayed in Fig. 3(c). These geometrical data are in close agreement with the van der Waals dimensions of pentacene and indicate a close packing of the planar molecules parallel to the sur-

face. Such an arrangement is in close agreement with the monolayer structure of pentacene on Au(111) reported previously by different groups.[27–29,43]

Attempts to also characterize the structure of the pentacene islands [denoted as II in Fig. 3(b)] by tunneling microscopy were not successful and are hampered by their low conductivity which prevents stable tunneling contacts even at currents as low as 10 pA. Corresponding *ex situ* AFM measurements yielded a typical island height of 30–50 nm.

B. SAM-covered gold surfaces

The initial film growth observed for noncleaned Au/mica substrates suggests that surface impurities severely affect the dewetting and the resulting film morphology. In order to provide a more defined modification of the substrate surface and to suppress any direct contact of the impinging pentacene molecules with the bare metal surface additional films were grown on a gold substrate that was first covered with a monolayer of decanethiol.

The resulting structure and morphology of a nominal 4 nm pentacene film deposited at room temperature on such a thiolated Au/mica surface are summarized in Fig. 4. The SEM micrographs reveal the presence of adjoined islands with typical lateral dimensions of 0.5–2 μm. Moreover, the corresponding STM data show that these islands consist of very smooth terraces and exhibit a distinct layer structure. From line scans a step height of $\Delta d=1.6\pm0.3$ nm was derived which agrees well with the interlayer distance $d_{(001)}$ in pentacene bulk crystals (see Fig. 1). By using tunneling currents as low as 15 pA the molecular structure of the individual layers could be resolved up to the fifth layer. As shown in Figs. 4(d) and 4(e) close-packed films with a char-
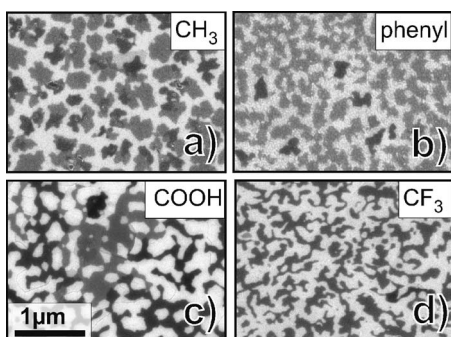
FIG. 5. SEM micrographs of nominal 2 nm pentacene films grown at 300 K (1.5 nm/min) onto thiolated Au(111)/mica substrates using SAM's with different terminations (a) C18-, (b) TP4-, (c) AcT-, and (d) FT-SAM's. All images are shown in the same magnification.

acteristic herringbone arrangement of pentacene molecules were observed in all these planes and yield a unit cell given by $\mathbf{a}=6.5\pm0.3$ Å and $\mathbf{b}=7.4\pm0.3$ Å with an included angle of about 85°. This structure is in close agreement with the molecular arrangement of pentacene in the *ab* plane of the bulk lattice shown in Fig. 1(a). Therefore we conclude that the molecular structure of these islands resembles that of (001)-oriented pentacene crystals. No further morphological change was observed over a period of several days when keeping this pentacene film under UHV conditions.

At this point we would like to emphasize that molecular resolution in the STM images of such multilayer films was only achieved at extreme low tunneling currents. In contrast, when using larger tunneling currents of about 0.5 nA or more the tip dips into the organic film during stabilization and occasionally yielded a distorted image of the SAM on the gold surface. Additional SEM and AFM measurements on pentacene/SAM films which were stored in air for several weeks revealed no morphological changes. We note further that molecular steps at such films could also be imaged by tapping-mode AFM under ambient conditions whereas a lateral resolution of closely packed molecules within the terraces could only be achieved for films which had not been exposed to air. If the pentacene films were imaged by SEM at high magnification (field of view typically less than $1~\mu\mathrm{m}^2$), a characteristic bleaching of the contrast was observed within a few seconds. Subsequent STM measurements on these intensely exposed areas allowed no longer molecular resolution and hence indicate the presence of radiation damages.

Since surface properties of SAM-modified substrates such as the degree of hydrophobicity are essentially determined by their chemical termination, it poses the question whether these end groups also affect the growth and morphology of pentacene films. Previous experiments by Hu *et al.*[30] indicated that pentacene molecules grow in a nearly upright orientation on SAM-covered gold surfaces independently of the actual SAM termination. To complement their experiments we have also characterized the morphology of thin pentacene films grown on Au/mica substrates precovered with SAM's of different chemical terminations. Figure 5 depicts a series of typical *ex situ* SEM micrographs taken for 2 nm pentacene

films. While some differences in the island shape are visible, all films reveal a substantially larger degree of wetting compared to pentacene films grown on a bare gold surface (see Fig. 3). The presence of less compact pentacene islands in case of the fluorinated (CF_3) and carboxilic acid (COOH) terminated SAM's can be related to a reduced ordering and a large number of domain boundaries within these SAM's which may affect the subsequent pentacene film growth. The different gray scales in the micrographs indicate the presence of distinct molecular layers. In fact, additional STM data which were recorded *in situ* for pentacene films on phenyl- and alkyl-terminated SAM's revealed the same molecular layer structure with the characteristic step height as shown in Fig. 4. This molecular orientation is further confirmed by our NEXAFS measurements for pentacene films deposited on all differently terminated SAM's (presented below).

So far we have considered only single-crystalline gold surfaces whereas typical electrodes in electronic devices are polycrystalline. In order to validate our previous results and to investigate the influence of substrate roughness on the growth properties and the resulting film morphology additional pentacene films were grown on polycrystalline gold substrates. For this purpose we have used gold films grown on silicon wafers which reveal typical grain sizes of 50–100 nm. Moreover, to provide a reliable comparison with the aforestudied Au(111) substrates the polycrystalline samples were either cleaned *in situ* by sputtering prior to the pentacene deposition or precovered with a C18-SAM.[41]

The resulting morphologies obtained for a 2 nm pentacene film deposited on differently treated polycrystalline gold substrates are compared in Fig. 6. In the case of a clean Au/Si substrate dark patches with typical diameters of $2-3~\mu\mathrm{m}$ surrounded by bright, nearly uncovered regions were observed in the SEM micrographs. A closer analysis based on high-resolution SEM and AFM measurements showed that these patches actually consist of several closely spaced tall pentacene islands with lateral dimensions of about 100–300 nm and a height of up to 20 nm which cover individual grains of the gold substrate [see the inset in Fig. 6(a)]. This demonstrates that also on polycrystalline gold substrates the morphology of pentacene films is largely affected by a pronounced dewetting. However, due to the large number of grain boundaries on these substrates, the effective diffusion length is significantly reduced. A statistical analysis of the AFM data yielded a root-means-square (rms) value for the roughness of 6.6 nm. In contrast to that distinctly smoother pentacene films are obtained for the thiolated Au/Si substrate. Instead of tall, nonconnected pentacene islands, small but smooth terraces of about 100 nm are observed and yield an rms value of the total roughness of only 1.1 nm.

C. Influence of growth rate and substrate temperature on morphology

Next the morphology of thicker pentacene films was studied. For this purpose films with a nominal thickness of about 30 nm were grown on the various gold substrates, and moreover, the influence of deposition rate and substrate temperature was investigated. Figure 7 summarizes typical SEM mi-
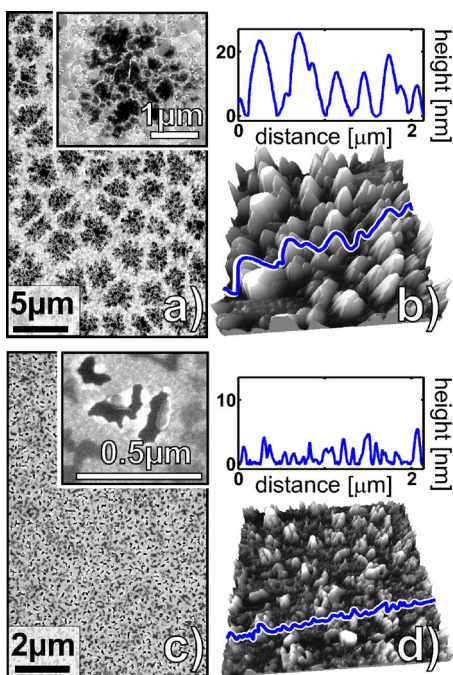
FIG. 6. (Color online) SEM micrographs and AFM data showing the morphology of 2 nm pentacene films grown at 310 K (0.6 nm/min) on polycrystalline Au/Si substrates (a), (b) on a clean surface and (c), (d) on an C18-SAM-covered surface.

crographs obtained for the different substrates and growth conditions.

Similar to the early stage of film growth on clean Au(111) surfaces (see Fig. 3) also the later growth is mainly governed by a pronounced dewetting which results in a network of individual, elongated crystallites [see Figs. 7(a)–7(c)]. The actual size of the crystallites and their separation depends on the deposition rate and temperature. Larger crystallites were observed either upon deposition at elevated temperature or low deposition rate. This can be attributed to an enhanced molecular diffusion rate relative to the nucleation rate which causes a ripening of individual crystallites. Note that due to a reduced sticking coefficient at elevated substrate temperatures, the actual coverage might be smaller than the nominal film thickness. Attempts to further characterize these pentacene films by means of AFM were not successful because the closely spaced, tall crystallites with a height exceeding more than 100 nm cannot be imaged without tip artifacts.

In contrast rather homogeneous pentacene films were obtained after deposition onto a SAM-covered Au/mica substrate for all studied deposition parameters [Figs. 7(d)–7(f)]. No distinct islands or crystallites are visible in the corresponding SEM and AFM data which instead reveal only small spots with lateral dimensions of 50–100 nm, indicating the presence of terraces of equal film height. The quantitative analysis of the AFM data yielded rms values of the roughness of 4–5 nm.

Deposition of pentacene onto clean, polycrystalline gold surfaces results in continuous but rough films. They exhibit further characteristic trenches which can be attributed to grain boundaries between initially formed crystallites [see Fig. 6(a)]. From AFM data an rms roughness of 15–20 nm
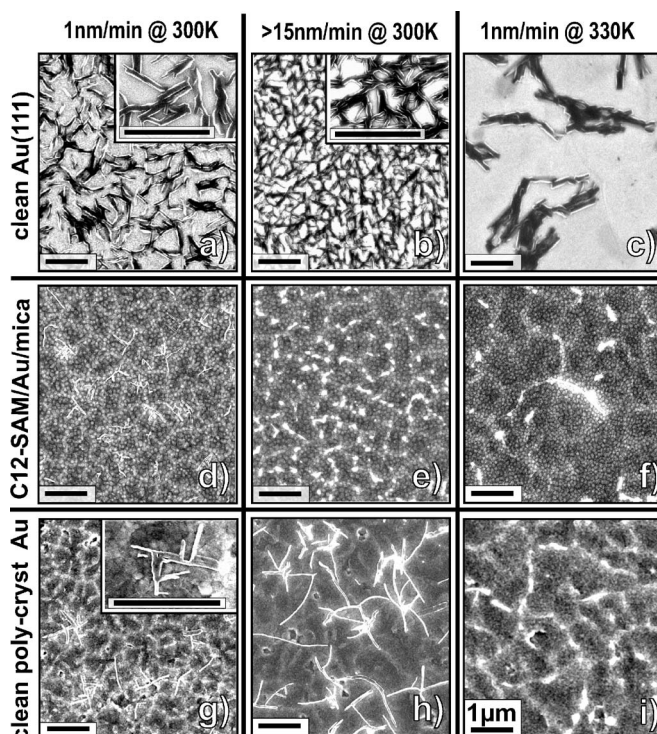

FIG. 7. Comparison of SEM micrographs obtained for 30 nm pentacene films grown (a)–(c) on clean Au(111), (d)–(f) on C12-SAM-covered Au/mica, and (g)–(i) on clean polycrystalline Au/Si. The films were grown at different deposition rates and temperature. Left column: 1 nm/min at 300 K. Center column: 15 nm/min at 300 K. Right column: 1 nm/min at 330 K. The scale bar in each panel denotes 1 μm.

was obtained for room-temperature deposition while a slightly lower value of about 10 nm was derived for a film grown at 330 K.

Occasionally additional needlelike, branched islands appear on the surface of thick pentacene films. High-resolution SEM micrographs recorded after slow deposition at room temperature [see inset in Fig. 7(g)] indicate the presence of characteristic angles of about 85° between the branches. The close agreement with the angle γ between the lattice vectors **a** and **b** in the bulk structure (see Fig. 1) suggests the presence of crystallites exhibiting an *ab* plane. A similar island morphology has been observed before upon growth of other organic semiconductors such as tetracene[42] or perylene[23] and indicates a skeleton growth. When increasing the deposition rate these additional crystallites are less branched and become longer while they are not formed upon slow deposition at elevated temperature (1 nm/min at 330 K), hence indicating their metastable nature.

In the process of device fabrication pentacene films are frequently prepared at rather high deposition rates and at elevated temperature without any further substrate cleaning. Therefore we have also characterized the morphology of thick (about 110 nm) pentacene films that were rapid grown at 340 K and a rate of 120 nm/min onto Au/mica substrates without additional cleaning. The SEM micrograph presented in Fig. 8(a) indicates that such a preparation again results in a network of interwoven elongated crystallites. Compared to
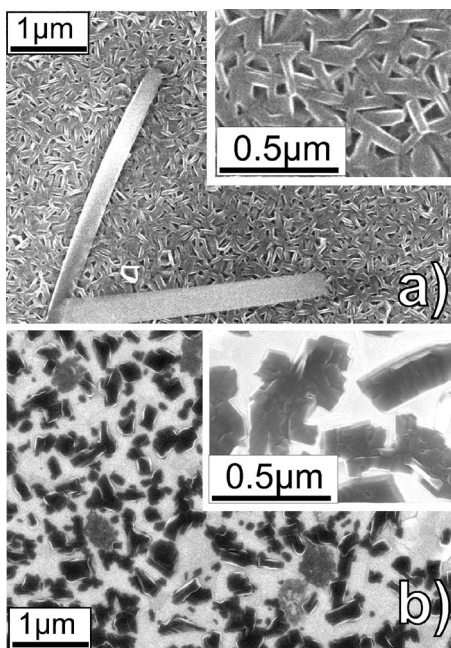
FIG. 8. SEM micrographs of thick (110 nm) pentacene films grown (a) on Au/mica as received (at 340 K, 120 nm/min) and (b) like (a) but after additional annealing at 370 K for 6 h under UHV conditions.

films grown on clean gold [see Figs. 7(a)–7(c)] the individual crystallites, however, appear to be more closely packed. In addition leaflike crystallites extending over more than 4 μm are formed, thus indicating an onset of three-dimensional (3D) crystal growth.

To study the affect of post-deposition annealing an identically prepared pentacene film was additionally heated at 370 K for 6 h under UHV conditions. Previous studies have shown that thermal desorption of pentacene does not occur at this temperature.[16] Subsequently recorded SEM micrographs reveal a complete change of film morphology which has transformed into nonconnected, compact crystallites with lateral dimensions of 200–300 nm as displayed in Fig. 8(b).

D. NEXAFS

To characterize the orientational order of pentacene in the differently prepared films systematic x-ray absorption spectroscopy measurements of the carbon K edge were carried out. To provide a reference system with a well-known geometrical structure at first NEXAFS spectra were recorded for a 65 nm pentacene film grown at room temperature on a SiO$_2$ substrate. As shown in Fig. 9(b) a common signature in the corresponding spectra are distinct sharp resonances at around 285 eV which are assigned to excitations of the C1s electrons into closely spaced unoccupied π^* orbitals. The broad resonances around 295 eV and 300 eV are attributed to excitations into σ^* orbitals.[44,45] To clarify the fine structure of the π^* resonances an enlarged view of this spectral region (283.0–287.5 eV) is displayed in the inset in Fig. 9(b). Clearly, the presence of at least seven distinct components at 283.73 eV, 284.25 eV, 284.68 eV, 285.20 eV, 285.77 eV,
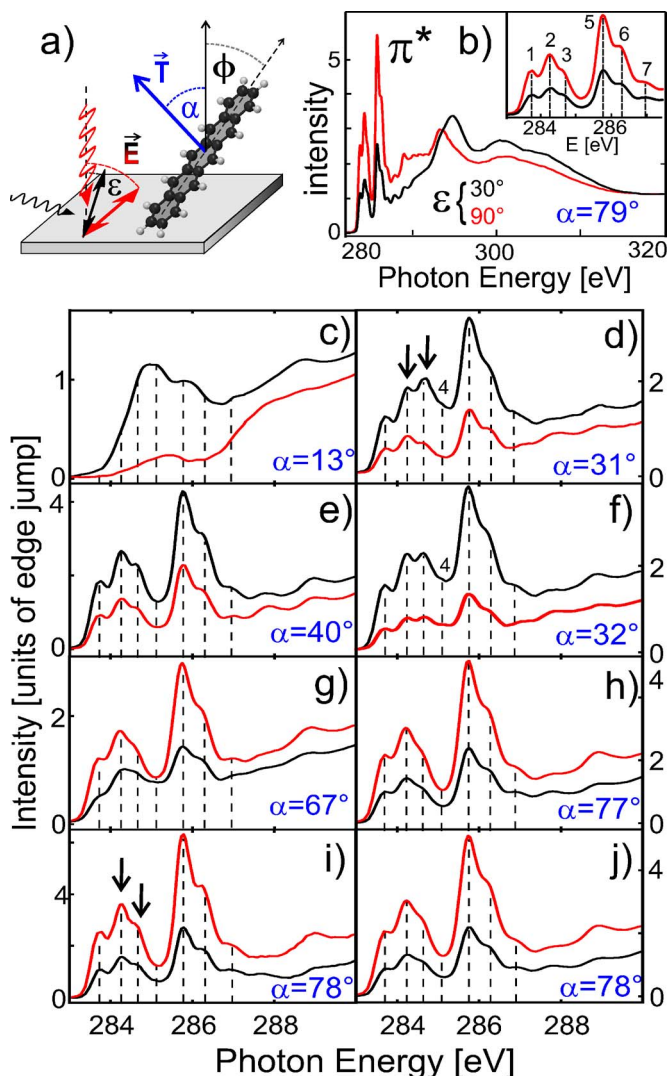

FIG. 9. (Color online) Series of typical C1s NEXAFS-spectra showing the π^* region for differently prepared pentacene films on the various gold substrates: (c) 0.4 nm on clean Au/mica (0.3 nm/min, at 310 K), (d) 20 nm on clean Au/mica (0.5 nm/min, at 300 K), (e) 110 nm on Au/mica (120 nm/min, at 340 K) [same sample as Fig. 8(a)], (f) identical deposition as (e) but after 6 h annealing at 370 K [same sample as in Fig. 8(b)], (g) 2 nm on clean polycrystalline Au/Si [0.6 nm/min, at 310 K; cf. Figs. 6(a) and 6(b)], (h) like (g) but 30 nm, (i) 25 nm on C12-SAM-covered Au/mica (0.6 nm/min, at 305 K), and (j) 30 nm on C12-SAM-covered Au/mica (16 nm/min, at 305 K). Additional C 1s NEXAFS spectra of a 65 nm pentacene film grown on SiO$_2$ (6.5 nm/min, at 300 K) are shown for comparison in panel (b) together with a magnification of the π^* region (inset). All spectra were recorded for various orientations of the electric field vector $\vec{E}$ parallel and upright to the surface by using different angles of incidence of the synchrotron light according to the experimental geometry [see panel (a)] which is denoted by the red ($\varepsilon=90°$) and black ($\varepsilon=30°$) curves, respectively.

286.26 eV, and 286.84 eV (labeled by 1–7) can be identified. Note that the fourth subresonance is only weak but can be seen more clearly in other spectra [cf. Fig. 9(f)]. This fine structure is in close agreement with previously reported

NEXAFS data of pentacene for its gas phase[46] or thin films grown on copper.[16]

Theoretical analyses based on *ab initio* calculations have shown that such a splitting results from initial-state effects due to slightly different chemical coordinations of the carbon atoms in the aromatic molecules (six nonequivalent C atoms are present in pentacene) as well as from final-state effects (caused by different positions of the core hole within the molecule).[45,46] The quantitative analysis shows further that the intensity of the π^* resonances depends on the relative orientation of the electrical field vector **E** of the incident synchrotron light and is given by $I_{\pi*} \propto |\mathbf{E} \cdot \mathbf{T}|^2$, where **T** denotes the transition dipole moment which is oriented normal to the ring plane of aromatic molecules.[47] For a substrate of threefold symmetry and linear polarized light with a degree of polarization P, this expression can be written as

$$I_{\pi*} \propto P \cos^2 \varepsilon \left(\frac{3 \cos^2 \alpha}{2} - \frac{1}{2} \right) + \frac{\sin^2 \alpha}{2},$$

where α and ε denote the angles between **T** and the surface normal and between **E** and the surface normal, respectively, as shown schematically in Fig. 9(a). Thus, from NEXAFS measurements for different angles of incidence of the incoming synchrotron light the average tilt angle of **T** relative to the sample normal, α, can be determined quantitatively. In the present study NEXAFS spectra have been recorded at least for three different angles of incidence $\varepsilon = 90°$ (denoted by red curves in Fig. 9), 55° (not shown), and 30° (black curves) for all films. To allow a more precise determination of the tilt angle specific films have been examined at six different angles of incidence.

The NEXAFS data of the pentacene film grown on SiO$_2$ reveal a pronounced dichroism of the π^* resonances which reflects a high degree of molecular orientation within the adlayer. A quantitative analysis of the resonance intensities $I_{\pi*}$ according to the above given equation yields an average tilt angle of the transition dipole moment of $\alpha = 79°$, thus indicating a nearly upright molecular orientation in the film.

Figures 9(c)–9(j) show a comparison of characteristic NEXAFS data which were chosen from more than 100 NEXAFS spectra obtained for the various pentacene films preparations on the different gold substrates. For clarification only the π^* region of each spectrum is shown and the intensity is given in units of the edge jump by normalizing the constant intensity after the edge jump at 325 eV to unity.

In contrast to all multilayer films only rather broad π^* resonances without any distinct fine structure were obtained for (sub)monolayer films of pentacene deposited on bare gold surfaces as shown for a Au/mica substrate in Fig. 9(c). The largest π^*-resonance intensity is measured for grazing incidence—i.e., at $\varepsilon = 30°$—and thus reveals a reversed dichroism as compared to SiO$_2$. A quantitative analysis yields an average tilt angle of $\alpha = 13°$ which is in agreement with a planar orientation suggested by the STM data of monolayer films presented above [see Fig. 3(c)]. A similar broadening has been observed before upon adsorption of pentacene and other planar aromatic molecules on various metal surfaces.[16–18] In that case the molecules adsorb with their ring plane parallel to the metal surface to maximize the elec-

tronic coupling of the aromatic system with the substrate.[47] In turn this causes a distortion and an energetic broadening of the molecular orbitals which also affects the orientation of the transition dipole moment and hence explains the deviation from a value of $\alpha = 0°$ expected for a planar adsorption.

For pentacene films grown on clean Au(111) substrates with thicknesses of more than 1–2 nm the NEXAFS spectra again exhibit distinct fine structures in the π^* region with a maximal intensity at grazing incidence (i.e., $\varepsilon = 30°$). Figure 9(d) displays a set of typical spectra of a 20 nm film grown on Au/mica (0.5 nm/min, at 300 K). No change in the spectral signature was observed with further increasing film thickness. The quantitative analysis of the dichroism yields an orientational angle of $\alpha = 31°$. We note that the same average tilt angle was also obtained for pentacene films which had been deposited onto a clean Au(111) surface at cryogenic temperatures of less than 200 K and afterwards heated slowly to room temperature.

A similar NEXAFS signature was observed for thick films that were grown at significantly larger deposition rates. Typical spectra of a 110 nm pentacene film which was deposited at an extremely high rate of 120 nm/min onto Au/mica at 340 K are displayed in Fig. 9(e). From a quantitative analysis of the π^*-resonance intensities an average tilt angle of $\alpha = 40°$ was determined. Since a drastic change in the morphology of this films was observed after annealing (cf. Fig. 8), additional NEXAFS spectra were recorded after heating an identically prepared film for 6 h at 370 K under UHV conditions. Somewhat surprisingly, only small changes are seen in the corresponding NEXAFS data presented in Fig. 9(f) which essentially reveal a slightly enhanced dichroism yielding a reduced average tilt angle of $\alpha = 32°$.

In contrast, a strikingly different NEXAFS signature is observed for all pentacene multilayer films grown on polycrystalline gold substrates. In contrast to films which had been grown on clean, (single) crystalline gold substrates [see Fig. 9(d)–9(f)] the dichroism of the π^* resonances is now completely reversed and reveals the largest intensity for perpendicular incidence of the synchrotron light ($\varepsilon = 90°$) as shown in Figs. 9(g) and 9(h) for 2 nm and 30 nm films deposited onto clean polycrystalline Au/Si substrates (0.6 nm/min, at 310 K). The quantitative analysis of the dichroism yields for thin films an average tilt angle of $\alpha = 67°$ which increases to 77° for films exceeding a thickness of 10–15 nm.

Finally the molecular orientation in pentacene films evaporated onto SAM-covered gold substrates was characterized. For these measurements at first NEXAFS spectra of the carbon containing self-assembled monolayers were recorded and then used for substrate subtraction. Figure 9(i) displays a set of typical NEXAFS spectra obtained for a 25 nm pentacene film grown on a C12-SAM covered Au/mica substrate which resemble the data obtained before for pentacene on SiO$_2$ [see Fig. 9(b)] and yielded an average angle of $\alpha = 78°$. To study also the influence of growth rate on the resulting molecular orientation for pentacene films on SAM-covered substrates additional films were grown with a deposition rate of 16 nm/min. As displayed in Fig. 9(j) these films reveal virtually an identical NEXAFS signature. Moreover, the same average orientational angles of $\alpha = 78°$ was

also obtained for pentacene films which were grown on differently terminated SAM's and at various deposition rates.

The quantitative analysis of the dichroism revealed a uniform angular dependency of all subresonances in each studied film according to the above given intensity variation $I_{\pi^*}(\varepsilon)$ expected for vector type orbitals[47] and thus confirms their assignment to π^* resonances. Therefore all subresonances have actually been used to determine the average tilt angle of the transition dipole moment, α, which improves the quality of the fit and provides an accuracy of about $\pm 3°$.

Note that the presently measured high-resolution NEXAFS data of multilayer films with differently oriented pentacene molecules allow further an additional characterization of the π^* subresonances. A closer comparison of the NEXAFS spectra reveals a distinct intensity variation of the third subresonance (π_3^*) relative to the other subresonances which depends on the molecular orientation: for upright-oriented molecules this subresonance is less intense while it is most intense for less-tilted pentacene [cf. arrows in Figs. 9(d) and 9(i)]. A previous theoretical analysis of the π^* resonances of pentacene by Alagia *et al.* indicates that the π_3^* resonance corresponds to a core-hole excitation within the outermost aromatic ring.[46] In case of an upright orientation this leads to a partial attenuation of the measured secondary electrons emitted from the lowest aromatic ring through the molecule which is consistent with the experimental observation.

Finally, we note that compared to *in situ*–prepared films no substantial differences were observed in the NEXAFS data of films that had been exposed to air for about 1 day [cf, for example, Figs. 9(h)–9(j)].

E. X-ray diffraction

To complement our structural characterization and to identify the crystalline phases and lattice parameters of pentacene films grown on highly crystalline Au(111)/mica substrates they have been further analyzed by *ex situ* XRD measurements. $\theta/2\theta$ scans of the bare Au/mica substrates were used for background subtraction to emphasize the pentacene-related diffraction peaks. Moreover, the characteristic (111) reflex of gold at $38.17°$ (corresponding to $d_{(111)} = 2.356$ Å) was used as an intrinsic reference to compensate possible angular offsets of the diffractometer.

Figure 10(a) displays an angular scan of a 170 nm pentacene film grown on a clean Au/mica substrate which reveals the presence of four distinct reflexes at $24.14°$, $25.73°$, $26.77°$, and $28.53°$ with corresponding interplanar spacings of 3.68 Å, 3.46 Å, 3.33 Å, and 3.13 Å, respectively. Using the pentacene bulk structure reported by Siegrist *et al.*[6] and calculating the expected reflex positions allows an indexing of the measured XRD pattern and yields (022), (121), (122), and (12$\bar{1}$) diffraction peaks with the (122) peak being the most intense one. We note that the differences between the calculated and measured peak positions correspond to maximal differences in the molecular plane distances of less than 0.05 Å compared to the bulk phase. This indicates that pentacene films grown on Au(111) substrates adopt a bulklike crystal phase. A comparison with XRD data obtained for a thinner pentacene film of only 30 nm reveals a similar dif-
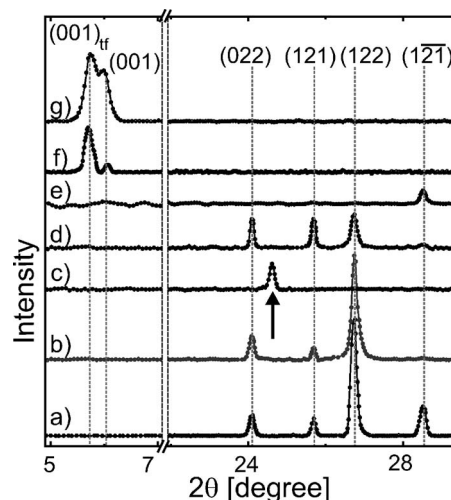

FIG. 10. $\theta/2\theta$ scans of differently prepared pentacene films: (a) 170 nm on clean Au/mica (1.5 nm/min, 300 K), (b) 30 nm on clean Au/mica (1.5 nm/min, 300 K), (c) 110 nm on Au/mica [120 nm/min, at 340 K; cf. Fig. 8(a)], (d) identical deposition as (c) but after 6 h annealing at 370 K [cf. Fig. 8(b)], (e) 30 nm on Au/mica as received (2 nm/min, 300 K), (f) 30 nm on C18-SAM/Au/mica (1.5 nm/min, 300 K), and (g) 65 nm on SiO$_2$ (6.5 nm/min, 300 K).

fraction pattern but without a (12$\bar{1}$) peak as shown in Fig. 10(b). Although the morphology of these films is generally dominated by a pronounced dewetting [see Figs. 7(a) and 7(b)], the absence of the (12$\bar{1}$) reflex suggests that this specific crystalline orientation develops only at larger film thicknesses.

On the other hand, a rather different crystalline phase was observed if the film had been grown at very high deposition rates of 120 nm/min. For this sample whose morphology is displayed in Fig. 8(a) only one diffraction peak was observed in the angular scan at an angle of $24.72°$ [indicated by the arrow in Fig. 10(c)] which corresponds to an interlayer spacing of 3.60 Å. While this diffraction peak suggests the presence of a new crystalline phase, it is only metastable and disappears completely upon annealing at 370 K. Subsequently recorded XRD data [see Fig. 10(d)] again reveal the presence of characteristic (022), (121), and (122) reflexes and thus parallels the structure observed before for thin films that were grown at low deposition rates on clean Au/mica [see Fig. 10(b)].

The aforerepresented delayed dewetting of thin pentacene films on non-UHV-cleaned gold substrates (see Sec. III A) suggests a strong influence of the surface cleanliness on the growth properties which is also reflected in the resulting crystalline phase. After deposition of 30 nm pentacene on a Au/mica surface which was not cleaned before deposition only a weak (11$\bar{2}$)-diffraction peak is seen in the corresponding x-ray diffraction pattern [see Fig. 10(e)]. Interestingly, the same crystalline orientation was found to develop at larger film thicknesses when the gold surface is already covered [cf. Figs. 10(a) and 10(b)] and thus suggests that this particular crystalline orientation is not mediated by the bare Au(111) surface.

Rather different diffractograms were obtained for pentacene films grown on SAM-covered Au/mica substrates. In

that case two distinct diffraction peaks at 5.69° and 6.05° were identified corresponding to interlayer spacings of 15.52 Å and 14.61 Å, respectively, as shown in Fig. 10(f). Very similar x-ray scans have also been recorded for pentacene films grown on SiO$_2$ [see Fig. 10(g): 5.74° and 5.99° corresponding to $d=15.39$ Å and 14.75 Å] which were additionally characterized as a reference system throughout this study. Such diffraction peaks have been observed before and were assigned to the (001) reflex of the well-known thin- and bulklike thick-film phases of pentacene formed on SiO$_2$.[12,13]

IV. DISCUSSION

By combining various microscopy techniques (STM, AFM, SEM) with x-ray diffraction and NEXAFS spectroscopy the molecular orientation, microstructure, and morphology of pentacene films developing upon deposition on gold substrates have been characterized in detail. A rather complex film growth was observed which depends critically on the surfaces properties of the gold substrates such as roughness and cleanliness while the deposition parameters (rate and temperature) were found to be less important.

On clean Au(111) substrates (single crystal or Au/mica) pentacene forms at first an ordered monolayer which is characterized by an adsorption geometry of the aromatic ring system oriented parallel to the substrate surface determined from the NEXAFS measurements. Corresponding STM data exhibit a characteristic side-by-side arrangement of the molecules with a close packing according to the van der Waals dimensions of pentacene. Such an adlayer structure is in close agreement with previously reported works[27–29] and appears in at least three rotational domains corresponding to the symmetry of the Au(111) substrate. The planar adsorption geometry enables a maximal electronic interaction of the molecular π system with the substrate. This is evidenced by the pronounced broadening of the individual π^* subresonances in the NEXAFS spectra which further reveal distinct shifts compared to their positions in the multilayers [indicated by the dashed lines in Fig. 9(c)].

The further growth of pentacene at *normal* deposition rates (i.e., less than about 25 nm/min) is characterized by a poor wetting of the chemisorbed first monolayer which causes the formation of nonconnected islands. The present SEM and AFM data show that such a dewetting occurs already upon deposition of pentacene films as thin as 2 nm and leads to distinct islands with a height of more than 50 nm. Previous growth experiments have further shown that such a dewetting occurs also upon thawing pentacene films which had been deposited at cryogenic temperatures[17] and thus can be related to the large mobility (diffusion) of pentacene molecules at room temperature.

While the surfaces of the individual islands are very flat as indicated by AFM measurements and occasionally reveal the presence of steps with a height of less than about 1 nm which can be related to molecular planes, the overall film roughness is very high. Corresponding XRD measurements indicate a highly crystalline ordering of such islands which reveal a preferential orientation of the (011), (121), (122), or (12̄1) planes parallel to the gold surface as depicted sche-
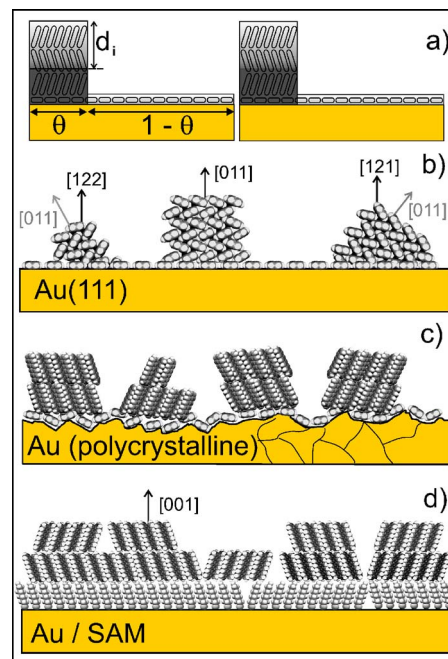

FIG. 11. (Color online) Schematic summary of the different film structures of pentacene growth on various gold substrates: (b) clean Au(111) (single crystal or Au/mica), (c) polycrystalline gold (e.g., Au/Si), and (d) SAM-covered gold. The observed dewetting reduces the effective surface covering as shown in (a).

matically in Fig. 11(b). Note that the close agreement of the molecular plane distances derived from x-ray diffraction scans of the films and the pentacene bulk structure[6] indicates the presence of a bulklike crystal phase without a polymorphism.

The quantitative analysis of the dichroism observed in the C1s NEXAFS spectra of thick pentacene films grown on clean Au(111) substrates yields an average orientation of the molecular transition dipole moment of $\alpha=31°$ relative to the sample normal. Because the transition dipole moment is oriented perpendicular to the aromatic ring plane, this angle also describes the tilt between the ring plane and the surface plane. Attempts to also determine precisely the individual molecular orientation are frequently complicated by the presence of differently oriented molecules in the crystalline packing or the presence of coexisting phases. Previously, we have demonstrated for the case of aromatic SAM's, where molecules adopt a herringbone arrangement, that the orientation of individual molecules can be deduced.[48]

We note further that under certain conditions also the film morphology has been taken into consideration when determining an average molecular orientation from the measured NEXAFS data. In the case of a pronounced dewetting the effective covering θ of the substrate—or in the present situation the first wetting layer—can be rather small even for multilayers as shown schematically in Fig. 11(a). This causes an overemphasis of the NEXAFS signal of the wetting layer (especially at perpendicular incidence) and thus affects the weighting of the relative resonance intensities measured for the different angles of incidence. On the other hand, due to the rather small probe depth of $d_i \approx 5$ nm seen by NEXAFS

when using a partial electron yield detection mode,[49] this effect becomes important only for very thin films. However, it explains the apparent continuous shift of the average tilt angle observed with increasing pentacene film thickness on clean Au(111) until a value of $\alpha = 31°$ is obtained for all films with nominal thicknesses larger than about 20 nm. In fact, a change in the tilt angle and the evolution of the fine structure in the π^* region for films exceeding the first monolayer on clean gold indicates an immediate change of orientation in the second monolayer. A similar scenario has been observed also for pentacene on Cu(110) where molecules continue to grow in a tilted fashion from the second layer on.[16] By using the distinct orientations of all pentacene crystallites identified in our XRD measurements and considering the molecular packing within each of these lattice planes according to the bulk crystal structure an average tilt angle of the aromatic ring planes relative to the surface plane of 34° was calculated. This value is in close agreement with an angle of $\alpha = 31°$ derived from the present NEXAFS measurements.

The present results of the structure of pentacene films on Au(111) are in pronounced variance with a planar stacking reported by Kang and Zhu.[29,43] In this context we again stress that imaging of weakly bound molecular multilayer films by means of STM is rather difficult and requires extremely low currents (as shown in Fig. 3). In a previous study on the growth of perylene, another planar aromatic molecule, on copper and gold surfaces we have demonstrated that imaging of multilayers is easily affected by the STM tip, leading to an imaging of the first monolayer only.[23]

A new, metastable crystal structure is observed after fast deposition of pentacene on gold at extremely high deposition rates of 120 nm/min. Although such films again reveal a netlike morphology [see Fig. 8(a)], the corresponding XRD diffraction pattern exhibits only one Bragg peak with a corresponding interlayer distance of 3.60 Å which is not included in the powder spectrum of the bulk structure of pentacene and thus indicates a new crystal phase. Corresponding NEXAS spectra reveal a somewhat smaller dichroism which yields an average tilt angle of $\alpha = 40°$. Combining the results of these two complementary techniques thus suggests a lower degree of molecular ordering which is consistent with a larger fraction of amorphous pentacene within the films and leads to a shift of the average tilt angle towards the magic angle of 55°. Upon extended heating at 370 K the film morphology changes and characteristic blocklike crystallites are formed. This change is accompanied by a reappearance of typical bulklike Bragg peaks as well as a reduction of the average tilt angle to $\alpha = 32°$ and reflects a recrystallization of the fast-grown, metastable film phase into the thermodynamically stable pentacene film structure on Au(111).

Interestingly, a distinctly different film structure is observed if pentacene was deposited onto clean, but polycrystalline gold substrates. The morphology of thin films is again characterized by a pronounced dewetting [see Fig. 6(a)]. However, the large number of grain boundaries and crystallites of the substrate limits the effective diffusion of pentacene. From the size of the characteristic halos surrounding the pentacene islands an effective diffusion length of about

$1-2$ μm can be estimated. Upon further deposition a coalescence of pentacene islands takes place, resulting in continuous but polycrystalline and rough films [see Figs. 7(g) and 7(h)]. Since the use of XRD to characterize the crystalline orientation of such pentacene films is hampered by the polycrystalline substrates, the molecular orientation was determined by NEXAFS. Initially, the molecular tilt angle slightly increases with the film thickness and again indicates the presence of a wetting layer of flat lying molecules. When increasing the nominal film thicknesses to more than 20 nm where the above-mentioned weighting effects can be excluded a constant average tilt angle of $\alpha = 77°$ was obtained. This value is almost identical to that obtained for pentacene films grown on SiO_2 and indicates the presence of nearly upright-standing molecules as shown schematically in Fig. 11(c).

By first coating Au(111) substrates with organothiol-based SAM's the formation of a chemisorbed wetting layer of flat lying pentacene molecules is suppressed and pentacene molecules grow in an upstanding orientation on the SAMs. In pronounced contrast to the above-discussed peculiarities of pentacene films on clean gold substrates the growth on SAM-pretreated gold surfaces proceeds in a quasi-layer-by-layer fashion and leads to rather smooth films. Especially, this enables the specific preparation of thin (001)-oriented crystalline islands, hence allowing a detailed characterization by STM. By using extremely low tunneling currents of only a few pA even the lateral molecular structure could be resolved up to the fifth monolayer and reveals a pentacene arrangement in close agreement with that present in the *ab* plane in the bulk structure [cf. Figs. 1(a) and 4(e)]. Whereas any attempts to characterize the tall pentacene islands formed spontaneously on clean gold by means of STM were hampered by their low conductivity, a detailed tunneling spectroscopic analysis was possible on the well-defined thin crystalline pentacene films on SAM-covered Au(111).[50]

More precise information about the crystalline structure of pentacene films on a SAM-covered Au(111) substrate has been derived from the corresponding XRD data. The two distinct (001) peaks which have been identified [see Fig. 10(f)] clearly reveal the presence of a thin-film and bulklike thick-film phase and hence parallels the structure of pentacene films on SiO_2. Previous experiments have shown that the ratio of both pentacene phases formed on SiO_2 can be largely controlled by the substrate temperature upon deposition[13] and especially allow a specific preparation of the thin film phase at reduced temperatures. Additional NEXAFS measurements that were carried out for a 9 nm pentacene film grown at 273 K onto SiO_2 (data not shown) yielded an average tilt angle of $\alpha = 85°$ for the thin-film phase. Considering further that pentacene molecules adopt a tilt angle of 73° relative to the *ab* plane in their bulk structure[6] an averaged tilt angle is expected for films revealing both phases. In particular, this explains the average tilt angle of $\alpha = 78°$ derived from the present NEXAFS measurements for the 30 nm pentacene film grown at room temperature on SiO_2. Very similar XRD and NEXAFS data were also obtained for pentacene films grown on the SAM-treated Au(111) substrate and thus suggest the same growth scenario. Note that the corresponding diffraction peak areas

clearly indicate the dominance of the thin-film phase while the present NEXAFS measurements are very surface sensitive due to the limited probe depth of only 5 nm for partial electron yield and thus overestimate the orientation within the top layers.

We note further that the molecular tilt angle in pentacene films is frequently derived from the interlayer separation measured by XRD and assuming a molecular stacking according to the van der Waals length of the molecule. A closer inspection of the crystal structure [see Fig. 1(b)] reveals, however, a small interdigitation of molecules between adjacent layers which needs to be considered. To provide also effective van der Waals dimensions of pentacene quantum chemical density functional theory (DFT) calculations were carried out by using the GAUSSIAN98 package[51] with a B3LYP/6-31+$G(d,p)$ basis set and a cutoff 0.02 and 98% electron density contours were used, yielding molecular box dimensions of 15.54 Å × 6.37 Å × 2.39 Å.

A strongly reduced film roughness is also observed for pentacene films grown on polycrystalline gold substrates which had been pretreated with a SAM (see Fig. 6). We note that this modified film growth is rather independent of the chemical termination of the SAM as well as the deposition rate which is in agreement with the results reported before by Hu *et al.*[30] In their study they used polycrystalline Au/Si substrates and observed a vertical layer spacing of $d_{(001)}$ = 15.3 Å for pentacene films grown on SAM-modified gold.

As regards the driving force for the diverse pentacene film structures formed on the different gold substrates we attribute this to a balanced interplay between a minimization of the surface free energy and a lattice constraint defined by the wetting layer. On chemically inert substrates (e.g., SiO_2, glass, or PTFE) as well as on silicon or metal surfaces which had been passivated by a molecular adlayer the mutual interaction among pentacene within the film dominates (or equals) the weak pentacene-substrate interaction (physisorption) and the film structure is governed by a minimization of the surface free energy which favors an (001) orientation.[11,30,33,52,53] In fact, theoretical analyses show that the (001) surface of pentacene crystals reveals the smallest free energy[54–56] and is also the dominating surface orientation observed in sublimation growth.[57] Frequently, also SiO_2 surfaces are coated by silane-based SAM's to improve the growth of pentacene films which has been attributed to a modification of surface energies and the hydrophobicity of the substrate.[58] We note, however, that pentacene and most other aromatic semiconductors are nonpolar molecules so that this interaction is less important which is also confirmed by the observed morphology of thin films grown on differently terminated SAM's (see Fig. 5).

Otherwise, on most single-crystalline metal surfaces planar aromatic hydrocarbons form a chemisorbed wetting layer of closely packed, flat-lying molecules. Considering further the characteristic face-on-edge herringbone arrangement adopted in the crystalline phase of these materials there exists no simple epitaxial relationship between the structure of the chemisorbed wetting layer and any lattice plane of the bulk structure. Therefore attempts to follow the newcrystalline packing introduced by the first monolayer will lead to a substantial misfit and strain between the first and second layer. It is most likely that the release of strain achieved by minimization of the contact area between the crystalline islands and the wetting layer is the driving force for the observed Stranski-Krastanov growth mode. This explains also the dewetting observed for pentacene films grown onto a long-range-ordered wetting layer—e.g., on Au(110).[59–61] Interestingly, all presently identified contact planes of the crystalline islands are characterized by a uniform orientation of the long axis of pentacene parallel to the surface, thus revealing a certain reminiscence of the wetting layer structure. Very similar microstructures have also been observed previously for pentacene films grown on Ag(111) (Ref. 62) and Cu(110) (Ref. 16) and hence suggest the same underlying growth mechanism. Only in rare cases such as, e.g., PTCDA/Ag(111) does the wetting layer provide a nearly perfect nucleation layer for a heteroepitaxial film growth. With increasing thickness, however, a substantial strain is built up even in these films which again is released by the formation of individual compact crystallites above a certain film thickness or upon annealing.[20] The importance of a close structural match between the first monolayer and possible lattice planes within the organic crystal seems to be an important design concept and has also been utilized for a controlled film growth of other nonplanar organic molecules like thiophenes and paraphenylenes on various substrates—e.g., Cu(110) and TiO_2(110).[63] In contrast, on polycrystalline substrates no structural long-range-ordered nucleation layer is formed which could be transferred to multilayers so that the resulting film structure is only controlled by the surface free energy, leading again to preferentially (001)-oriented films. Similar effects have also been reported recently for the growth of pentacene on polycrystalline copper surfaces.[64] We thus expect the resulting molecular orientation to depend critically on the surface roughness and average crystallite size of the (metal) substrates.

Finally, we note that the presently observed dewetting of pentacene films grown on polycrystalline gold substrates has also a severe effect for device applications because it introduces a large number of grain boundaries and thus reduces the effective charge carrier mobility. A promising strategy to improve the morphology of the active semiconductor layer has been demonstrated recently by first covering the gold electrodes of an OFET by an aromatic SAM which causes an enhancement of the ON/OFF ratio by a factor of 10^4 (Ref. 65).

V. CONCLUSIONS

A systematic analysis of the structural and morphological evolution of pentacene films grown by molecular beam deposition onto various gold surfaces is presented. Already the initial stage of film growth on clean gold substrates of different degrees of crystallinity is characterized by a pronounced dewetting and is further accompanied by a molecular reorientation beyond the first monolayer. It is emphasized that this particular morphology has to be taken into consideration when assigning spectroscopic data recorded for thin films. The observed crystalline structure of all pentacene films is in close agreement with the bulk structure while the

crystalline orientation of the resulting islands depends sensitively on the microstructure of the substrate such as roughness and cleanliness, hence revealing distinct differences for single-crystalline and polycrystalline gold substrates. Finally, it is demonstrated that by first coating the gold substrates with an organothiol-based self-assembled monolayer the formation of a chemisorbed pentacene wetting layer is suppressed and the molecules grow in an upright orientation without any dewetting, leading to rather smooth films on all studied gold substrates.

*Electronic address: witte@pc.rub.de

[1] S. Forrest, P. Burrows, and M. Thompson, IEEE Spectrum **37**, 29 (2000).

[2] J. M. Shaw and P. F. Seidler, IBM J. Res. Dev. **45**, 3 (2001).

[3] C. D. Dimitrakopoulos and P. R. L. Malenfant, Adv. Mater. (Weinheim, Ger.) **14**, 99 (2002).

[4] D. J. Gundlach, Y. Y. Lin, T. N. Jackson, S. F. Nelson, and D. G. Schlom, IEEE Electron Device Lett. **18**, 87 (1997).

[5] H. Klauk, M. Halik, U. Zschieschang, G. Schmid, W. Radik, and W. Weber, J. Appl. Phys. **92**, 5259 (2002).

[6] T. Siegrist, C. Kloc, J. H. Schön, B. Batlogg, R. C. Haddon, S. Berg, and G. A. Thomas, Angew. Chem., Int. Ed. Engl. **40**, 1732 (2001).

[7] The structural analysis of Siegrist and co-workers (Ref. 6) yielded unit cell vectors a=6.265 Å, b=7.786 Å, and c=14.511 Å with the corresponding angles α=76.65°, β=87.50°, and γ=84.61°. Note that slight variations of this structure have been reported which are usually attributed to the presence of polymorphism, although crystals have been grown in part by rather different techniques involving vacuum sublimation and solution growth.

[8] N. Karl, Synth. Met. **133-134**, 649 (2003).

[9] J. Cornil, J. P. Calbert, and J. L. Bredas, J. Am. Chem. Soc. **123**, 1250 (2001).

[10] G. Witte and Ch. Wöll, J. Mater. Res. **19**, 1889 (2004).

[11] S. E. Fritz, S. M. Martin, C. D. Frisbie, M. D. Ward, and M. F. Toney, J. Am. Chem. Soc. **126**, 4084 (2004).

[12] C. D. Dimitrakopoulos, A. R. Brown, and A. Pomp, J. Appl. Phys. **80**, 2501 (1996).

[13] I. P. M Bouchoms, W. A. Schoonveld, J. Vrijmoeth, and T. M. Klapwijk, Synth. Met. **104**, 175 (1999).

[14] E. Umbach, M. Sokolowski, and R. Fink, Appl. Phys. A: Mater. Sci. Process. **63**, 565 (1996).

[15] L. Casalis, M. F. Danisman, B. Nickel, G. Bracco, T. Toccoli, S. Iannotta, and G. Scoles, Phys. Rev. Lett. **90**, 206101 (2003).

[16] S. Söhnchen, S. Lukas, and G. Witte, J. Chem. Phys. **121**, 525 (2004).

[17] G. Beernink, T. Strunskus, G. Witte, and Ch. Wöll, Appl. Phys. Lett. **85**, 398 (2004).

[18] K. Hänel, S. Söhnchen, S. Lukas, G. Beernink, A. Birkner, T. Strunskus, G. Witte, and Ch. Wöll, J. Mater. Res. **19**, 2049 (2004).

[19] S. Mülleger, I. Salzmann, R. Resel, G. Hlawacek, C. Teichert, and A. Winkler, J. Chem. Phys. **121**, 2272 (2004).

[20] B. Krause, A. C. Dürr, F. Schreiber, H. Dosch, and O. H. Seeck, J. Chem. Phys. **119**, 3429 (2003).

[21] L. Kilian, E. Umbach, and M. Sokolowski, Surf. Sci. **573**, 359 (2004).

[22] T. Wagner, A. Bannani, C. Bobisch, H. Karacuban, M. Stöhr, M. Gabriel, and R. Möller, Org. Electron. **5**, 35 (2004).

[23] G. Witte, K. Hänel, S. Söhnchen, and Ch. Wöll, Appl. Phys. A: Mater. Sci. Process. **82**, 447 (2006).

[24] P. G. Schroeder, C. B. France, J. B. Park, and B. A. Parkinson, J. Appl. Phys. **91**, 3010 (2002).

[25] N. Koch, A. Elschner, J. Schwartz, and A. Kahn, Appl. Phys. Lett. **82**, 2281 (2003).

[26] F. Amy, C. Chan, and A. Kahn, Org. Electron. **6**, 85 (2005).

[27] C. B. France, P. G. Schroeder, and B. A. Parkinson, Nano Lett. **2**, 693 (2002).

[28] C. B. France, P. G. Schroeder, J. C. Forsythe, and B. A. Parkinson, Langmuir **19**, 1274 (2003).

[29] J. H. Kang and X. Y. Zhu, Appl. Phys. Lett. **82**, 3248 (2003).

[30] W. S. Hu, Y. T. Tao, Y. J. Hsu, D. H. Wei, and Y. S. Wu, Langmuir **21**, 2260 (2005).

[31] F. Schreiber, Prog. Surf. Sci. **65**, 151 (2000).

[32] J. C. Love, L. A. Estroff, J. K. Kriebel, R. G. Nuzzo, and G. M. Whitesides, Chem. Rev. (Washington, D.C.) **105**, 1103 (2005).

[33] F. J. M. Z. Heringsdorf, M. C. Reuter, and R. M. Tromp, Nature (London) **412**, 517 (2001).

[34] K. P. Weidkamp, C. A. Hacker, M. P. Schwartz, X. P. Cao, R. M. Tromp, and R. J. Hamers, J. Phys. Chem. B **107**, 11142 (2003).

[35] H. Fukagawa, H. Yamane, T. Kataoka, S. Kera, M. Nakamura, K. Kudo, and N. Ueno, Phys. Rev. B **73**, 245310 (2006).

[36] T. Sato, S. Kitamura, and M. Iwatsuki, J. Vac. Sci. Technol. A **18**, 960 (2000).

[37] S. Reiss, H. Krumm, A. Niklewski, V. Staemmler, and Ch. Wöll, J. Chem. Phys. **116**, 7704 (2002).

[38] NIST X-ray Photoelectron Spectroscopy Database 20, version 3.4 (Web version), http://srdata.nist.gov/xps/

[39] G. Loepp, S. Vollmer, G. Witte, and Ch. Wöll, Langmuir **15**, 3767 (1999).

[40] D. Käfer and G. Witte, Phys. Chem. Chem. Phys. **7**, 2850 (2005).

[41] Note that the remaining impurities on the gold surface, which essentially consists of hydrocarbons, are effectively replaced by the covalently bond thiolate upon SAM formation.

[42] M. Voigt, S. Dorsfeld, A. Volz, and M. Sokolowski, Phys. Rev. Lett. **91**, 026103 (2003).

[43] J. H. Kang and X. Y. Zhu, Chem. Mater. **18**, 1318 (2006).

[44] T. Yokoyama, K. Seki, I. Morisada, K. Edamatsu, and T. Ohta, Phys. Scr. **41**, 169 (1990).

[45] H. Ågren, O. Vahtras, and V. Carravetta, Chem. Phys. **196**, 47

(1995).

[46] M. Alagia, C. Baldacchini, M. G. Betti, F. Bussolotti, V. Carravetta, U. Ekström, C. Marani, and S. Stranges, J. Chem. Phys. **122**, 124305 (2005).

[47] J. Stöhr, *NEXAFS Spectroscopy* (Springer, New York, 1992), Vol. 25.

[48] D. Käfer, G. Witte, P. Cyganik, A. Terfort, and Ch. Wöll, J. Am. Chem. Soc. **128**, 1723 (2006).

[49] D. Käfer, L. Ruppel, G. Witte, and Ch. Wöll, Phys. Rev. Lett. **95**, 166602 (2005).

[50] L. Ruppel, A. Birkner, G. Witte, C. Busse, T. Lindner, G. Paasch, and Ch. Wöll (unpublished).

[51] GAUSSIAN 98, revision A.11.1, Gaussian, Inc., Pittsburgh, PA, 2001.

[52] M. Brinkmann, S. Graff, Ch. Straupe, J. C. Wittmann, Ch. Chaumont, F. Nuesch, A. Aziz, M. Schaer, and L. Zuppiroli, J. Phys. Chem. B **107**, 10531 (2003).

[53] T. Minakata, H. Imai, M. Ozaki, and K. Saco, J. Appl. Phys. **72**, 5220 (1992).

[54] J. E. Northrup, M. L. Tiago, and S. G. Louie, Phys. Rev. B **66**, 121404(R) (2002).

[55] S. Verlaak, S. Steudel, P. Heremans, D. Janssen, and M. S. Deleuze, Phys. Rev. B **68**, 195409 (2003).

[56] L. F. Drummy, P. K. Miska, D. Alberts, N. Lee, and D. C. Martin, J. Phys. Chem. B **110**, 6066 (2006).

[57] R. W. I. de Boer, M. E. Gershenson, A. F. Morpurgo, and V. Podzorov, Phys. Status Solidi A **201**, 1302 (2004).

[58] T. W. Kelley, L. D. Boardman, T. D. Dunbar, D. V. Muyres, M. J. Pellerite, and T. P. Smith, J. Phys. Chem. B **107**, 5877 (2003).

[59] V. Corradini, C. Menozzi, M. Cavallini, F. Biscarini, M. G. Betti, and C. Mariani, Surf. Sci. **532**, 249 (2003).

[60] Ph. Guaino, D. Carty, G. Hughes, O. McDonald, and A. A. Cafolla, Appl. Phys. Lett. **85**, 2777 (2004).

[61] L. Floreano, A. Cossaro, D. Cvetko, G. Bavdek, and A. Morgante, J. Phys. Chem. B **110**, 4908 (2006).

[62] L. Casalis, M. F. Danisman, B. Nickel, G. Bracco, T. Toccoli, S. Ianotta, and G. Scoles, Phys. Rev. Lett. **90**, 206101 (2003).

[63] G. Koller, S. Berkebile, J. R. Krenn, F. P. Netzer, M. Oehzelt, T. Haber, R. Resel, and M. G. Ramsey, Nano Lett. **6**, 1207 (2006).

[64] M. Oehzelt, R. Resel, C. Suess, R. Friedlein, and W. R. Salaneck, J. Chem. Phys. **124**, 054711 (2006).

[65] C. Bock, D. V. Pham, U. Kunze, D. Käfer, G. Witte, and Ch. Wöll, J. Appl. Phys. **100**, 114517 (2006).